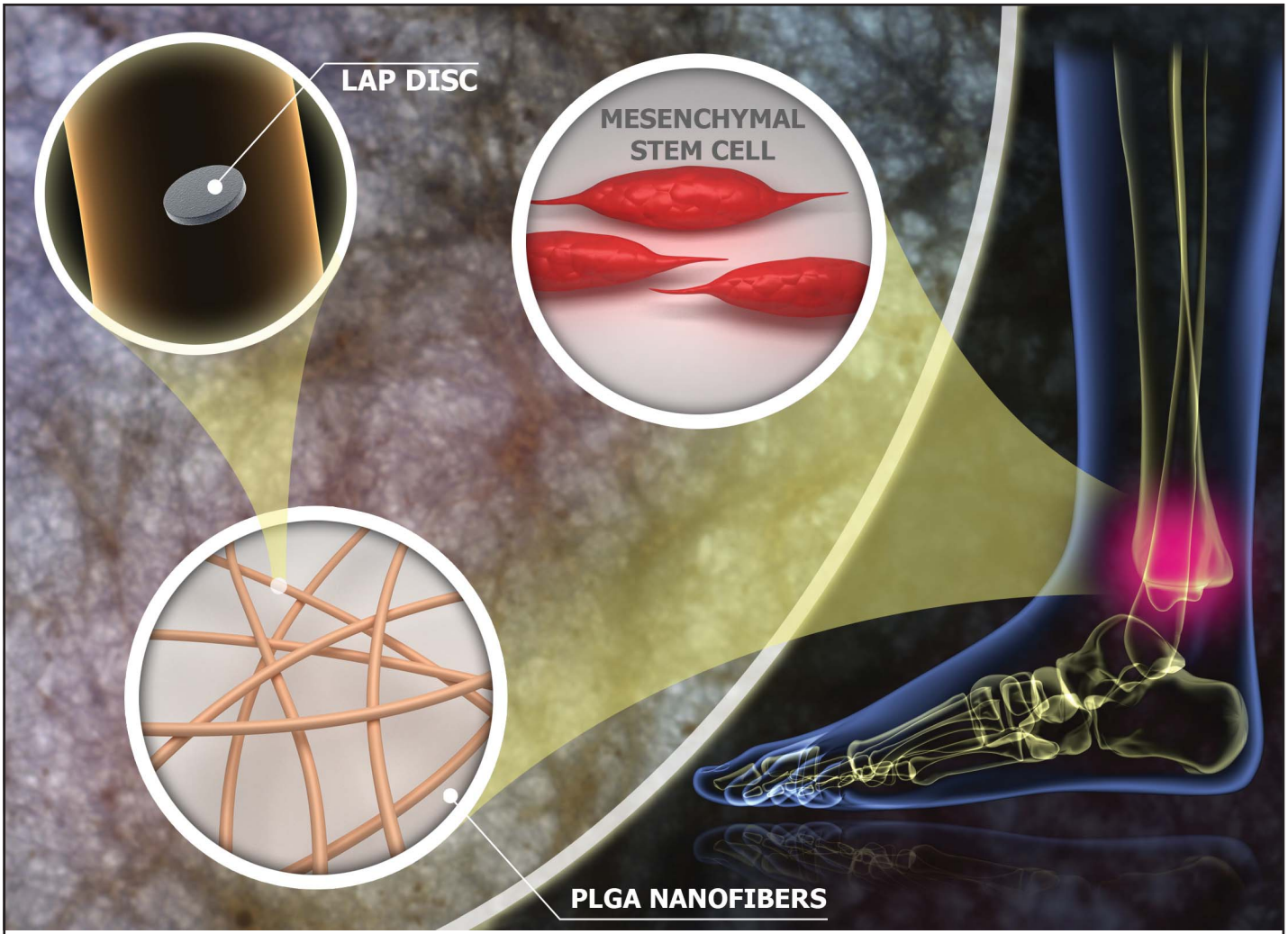


**Showcasing research from the College of Chemistry, Chemical Engineering and Biotechnology, Donghua University, Shanghai, China, in collaboration with colleagues at the Centro de Química da Madeira, Universidade da Madeira, Funchal, Portugal.**

**Title: Electrospun laponite-doped poly(lactic-*co*-glycolic acid) nanofibers for osteogenic differentiation of human mesenchymal stem cells**

We report the fabrication of uniform electrospun poly(lactic-co-glycolic acid) (PLGA) nanofibers incorporated with laponite (LAP) nanodisks for stem cell differentiation applications. Our results show that the doped LAP within the PLGA nanofibers is able to induce the osteoblast differentiation of human mesenchymal stem cells in growth medium without any inducing factors. The fabricated organic/inorganic hybrid nanofibers may find many applications in the field of tissue engineering.

## As featured in:

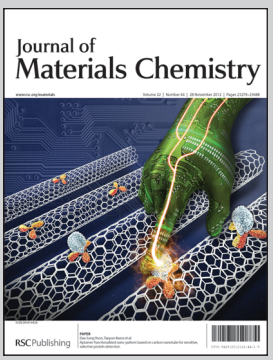


Helena Tomás, Xiangyang Shi *et al.*, *J. Mater. Chem.*, 2012, **22**, 23357.

RSC Publishing

**www.rsc.org/materials**

Registered Charity Number 207890

Journal of Materials Chemistry

Dynamic Article Links

Cite this: *J. Mater. Chem.*, 2012, **22**, 23357

www.rsc.org/materials

**PAPER**



# Electrospun laponite-doped poly(lactic-*co*-glycolic acid) nanofibers for osteogenic differentiation of human mesenchymal stem cells†

**Shige Wang,[ab] Rita Castro,[c] Xiao An,[d] Chenlei Song,[b] Yu Luo,[a] Mingwu Shen,[a] Helena Tomás,*[c] Meifang Zhu[b] and Xiangyang Shi*[abc]**

***Received 1st July 2012, Accepted 17th September 2012***
**DOI: 10.1039/c2jm34249a**

We report the fabrication of uniform electrospun poly(lactic-*co*-glycolic acid) (PLGA) nanofibers incorporated with laponite (LAP) nanodisks, a synthetic clay material for osteogenic differentiation of human mesenchymal stem cells (hMSCs). In this study, a solution mixture of LAP suspension and PLGA was electrospun to form composite PLGA–LAP nanofibers with different LAP doping levels. The PLGA–LAP composite nanofibers formed were systematically characterized *via* different techniques. We show that the incorporation of LAP nanodisks does not significantly change the uniform PLGA fiber morphology, instead significantly improves the mechanical durability of the nanofibers. Compared to LAP-free PLGA nanofibers, the surface hydrophilicity and protein adsorption capacity of the composite nanofibers slightly increase after doping with LAP, while the hemocompatibility of the fibers does not appreciably change. The cytocompatibility of the PLGA–LAP composite nanofibers was assessed by the 3-(4,5-dimethylthiazol-2-yl)-2,5-diphenyltetrazolium bromide (MTT) assay of L929 mouse fibroblasts and porcine iliac artery endothelial cells cultured onto the surface of the nanofibers. The results reveal that the incorporated LAP is beneficial to promote the cell adhesion and proliferation to some extent likely due to the improved surface hydrophilicity and protein adsorption capability of the fibers. Finally, the PLGA–LAP composite nanofibers were used as scaffolds for osteogenic differentiation of hMSCs. We show that both PLGA and PLGA–LAP composite nanofibers are able to support the osteoblast differentiation of hMSCs in osteogenic medium. Most strikingly, the doped LAP within the PLGA nanofibers is able to induce the osteoblast differentiation of hMSCs in growth medium without any inducing factors. The fabricated smooth and uniform organic–inorganic hybrid LAP-doped PLGA nanofibers may find many applications in the field of tissue engineering.

## Introduction

Hybrid nanofibers in general refer to fibers that consist of different components.[1–6] The existence of multiple components within the hybrid nanofibers enables the fibers with desired functionality and improved properties for many different applications. For instance, zero-valent iron nanoparticle (NP)-immobilized polyacrylic acid (PAA)–polyvinyl alcohol (PVA) nanofibers display superior environmental remediation capability.[7–12] Metal gold or palladium NP-immobilized polyethyleneimine (PEI)–PVA nanofibers are able to be used as highly efficient and reusable catalysts.[13,14] Similarly, hybrid nanofibers have also been used to encapsulate drugs for sustained release with improved release profiles.[15–17] With a judicious design of the hybrid nanofiber system, the fibers can be endowed with improved mechanical durability[18–20] or biocompatibility[21–24] that allows the cells to be well attached and proliferated. Therefore, hybrid nanofibers have generated great interest in the biomedical research areas such as tissue engineering[16,22,24] and drug delivery.[16,25]

Electrospinning has been considered as one of the most efficient techniques to fabricate continuous fibers with diameters ranging from tens of nanometers to a few micrometers.[26–28] For the generation of electrospun hybrid nanofibers, various approaches have been reported in the literature.[29] Hybrid nanofibers can be easily fabricated by electrospinning the

[a]*College of Chemistry, Chemical Engineering and Biotechnology, Donghua University, Shanghai 201620, People's Republic of China. E-mail: xshi@dhu.edu.cn*
[b]*State Key Laboratory for Modification of Chemical Fibers and Polymer Materials, Donghua University, Shanghai 201620, People's Republic of China*
[c]*CQM-Centro de Química da Madeira, Universidade da Madeira, Campus da Penteada, 9000-390 Funchal, Portugal. E-mail: lenat@uma.pt*
[d]*School of Medicine, Shanghai Jiaotong University Affiliated First People's Hospital, Shanghai Jiaotong University, Shanghai 200080, People's Republic of China*
† Electronic supplementary information (ESI) available: Additional experimental results. See DOI: 10.1039/c2jm34249a

solution mixture of two or more types of polymers or polymer/inorganic NPs.[2,21,30,31] In addition, precursors of the inorganic components can be electrospun with polymers to form blend fibers for subsequent reactions to generate the hybrid nanofibers.[32] Furthermore, preformed electrospun polymer-based nanofibers can be used as templates or reaction substrates that allow for various reactions or surface modifications to generate a wide range of hybrid nanofibers.[3,5,9,13,14] In other studies, it has been demonstrated that core–shell hybrid nanofibers with different components can be prepared *via* a coaxial electrospinning method.[33] It is generally accepted that a diversified range of functional components can be added to the electrospinning solution to obtain hybrid nanofibers with well-defined functionality *via* electrospinning.[34]

Laponite (LAP) is a kind of synthetic silicate clay material, consisting of disks of nanometric dimensions, and can degrade into non-toxic products.[35] By far, LAP has been incorporated into various polymers such as poly(ethylene oxide) (PEO) or chitosan to get hybrid hydrogels[36–38] or electrospun nanofibers.[39] For example, Gaharwar *et al.* reported the formation of PEO–LAP hydrogels for fibroblast attachment and proliferation with high cell viability.[36] Schexnailder *et al.* reported the control of cell adhesion through incorporating LAP into PEO hydrogels and found that fibroblast cells could not adhere to pure PEO hydrogels, but rather easily attached to the hybrid PEO–LAP hydrogels.[38] It is reasonable to expect that by incorporating LAP within electrospun polymer nanofibers, which can mimic the structure and biological function of the native extracellular matrix (ECM), improved cellular response may be achieved. Although Daga *et al.* reported the formation of PEO–LAP nanofibers and explored the relationship between the fiber morphology and solution properties,[39] the biocompatibility or cellular response of the hybrid LAP-based electrospun nanofibers has not been reported in the literature.

Human mesenchymal stem cells (hMSCs) are multi-potential stem cells which have an inherent ability to differentiate into many kinds of lineages, such as osteogenic,[40,41] chondrogenic,[42,43] myogenic,[44] adipogenic,[45,46] and neurogenic lineages.[47] The ECM mimicking property affords electrospun polymer nanofibers to be an ideal scaffold material for differentiation of hMSCs for various tissue engineering applications.[41] For example, Martins *et al.* reported that dexamethasone (DEX), an osteogenic inducing factor incorporated within electrospun polycaprolactone (PCL) nanofibers, was able to be released in a sustained mode over a period of 15 days and the electrospun DEX-incorporated PCL nanofibers were able to induce osteogenic differentiation of human bone marrow stem cells for bone tissue engineering applications.[48] Xin *et al.* found that electrospun PLGA nanofibers could serve as an accommodative milieu not only for hMSC differentiation, but also for the growth of hMSC-derived osteogenic and chondrogenic cells.[40] To our knowledge, there has been no study concerning the cellular response as well as the osteogenic differentiation of hMSCs on LAP-doped electrospun nanofibers.

In the present study, we prepared hybrid LAP-doped electrospun PLGA nanofibers and investigated the cellular response as well as the possibility of inducing the osteogenic differentiation of hMSCs using this hybrid nanofiber scaffold. The PLGA–LAP hybrid nanofibers were characterized *via* different techniques. The influence of the incorporated LAP on morphology, mechanical durability, and surface hydrophilicity of the hybrid fibers was systematically investigated using scanning electron microscopy (SEM), tensile test, and water contact angle test, respectively. The protein adsorption onto PLGA and LAP-doped PLGA nanofibers was quantified *via* UV-Vis spectrometry. The hemocompatibility of the LAP-doped PLGA nanofibers was evaluated *via* hemolytic and anticoagulant assays. The cytocompatibility of the as-prepared nanofibers was evaluated using the 3-(4,5-dimethylthiazol-2-yl)-2,5-diphenyltetrazolium bromide (MTT) assay as well as by the SEM morphological observation of L929 mouse fibroblasts and porcine iliac artery endothelial cells (PIECs) cultured onto the fibrous scaffolds. Finally, the metabolic activity of hMSCs cultured onto LAP-doped PLGA nanofibers was analyzed using the resazurin reduction assay, and their osteogenic differentiation was evaluated by quantitatively and qualitatively analyzing the cellular alkaline phosphatase (ALP) activity (an earlier marker of osteogenesis), and by measuring the cellular osteocalcin secretion (a later marker of osteogenesis).

## Experimental

### Materials

PLGA ($M_w$ = 81 000 g mol$^{-1}$) with a lactic acid–glycolic acid ratio of 50 : 50 was purchased from Jinan Daigang Bio-technology Co., Ltd. (China). LAP was friendly offered from Rockwood Additives Limited (UK). Tetrahydrofuran (THF), *N*,*N*-dimethyl formamide (DMF), dimethylsulfoxide (DMSO), silver nitrate, and sodium thiosulfate were from Sinopharm Chemical Reagent Co., Ltd. (Shanghai, China). L929 and PIECs were obtained from Institute of Biochemistry and Cell Biology (the Chinese Academy of Sciences, Shanghai, China). Small pieces of human bone marrow were obtained from healthy adults during surgical interventions after trauma. Only tissue that would have been discarded was used, with the approval of the *Região Autónoma da Madeira* (Portugal) Local Ethics Committee (Ref. 45/08, 14/07/2008). Eagle's Minimal Essential Medium (α-MEM), Dulbecco's Modified Eagle's Medium (DMEM), fetal bovine serum (FBS), phosphate buffer saline (PBS), penicillin, and streptomycin were purchased from Gibco (UK). DEX, β-glycerophosphate (β-GP), ascorbic acid, resazurin, *p*-nitrophenyl phosphate, and *p*-nitrophenol standard were from Sigma. $CaCl_2$, NaOH, and formaldehyde were from Merck. Reporter Lysis Buffer was from Promega (USA). The Picogreen DNA quantification kit was from Molecular Probes, Inc. (USA). The intact human osteocalcin EIA kit was from Biomedical Technologies Inc. (USA). The QuantiChrom Calcium Assay Kit was purchased from Bioassay Systems (Hayward, CA). Heparin stabilized human blood was kindly provided by Shanghai First People's Hospital (Shanghai, China). Water used in all experiments was purified using a Milli-Q Plus 185 water purification system (Millipore, Bedford, MA) with resistivity higher than 18 MΩ cm.

### Preparation of electrospun LAP-doped PLGA nanofibers

Following the procedures reported in our previous study,[16,20,21] PLGA was dissolved in a mixed solvent of THF–DMF

 

(v/v = 3 : 1) with magnetic stirring overnight to obtain a homogeneous solution with a concentration of 25% (w/v). After that, LAP (1, 3, and 5 wt% relative to PLGA, respectively) was added into the above PLGA solution, followed by continuous stirring for 30 min to obtain a homogeneous solution mixed with different amounts of LAP.

The electrospinning system consists of a syringe pump with a 10 mL syringe, a silicone hose, a stainless steel needle with an inner diameter of 0.8 mm, a high voltage power supply, and a thin aluminum foil acting as a collector which was positioned horizontally and grounded. A clamp was used to connect the high voltage power supply with the needle. A fixed electrical potential of 20 kV was employed to charge the steel capillary. The distance between the tip and the collector was set at 15 cm. The electrospinning solution was fed at a speed of 0.8 mL $h^{-1}$ by the syringe pump, and the electrospinning process was carried out under ambient conditions. After electrospinning, aluminum foil with the formed nanofibrous mat was taken off from the collector immediately and vacuum dried for at least 48 h to remove the residual organic solvent and moisture. Finally, the formed nanofibers were removed carefully from the aluminum foil and stored in a desiccator before use.

### Characterization techniques

The morphology of PLGA and LAP-doped PLGA nanofibers was observed using SEM (JEOL JSM-5600LV, Japan) with an accelerating voltage of 10 kV. All samples were sputter coated with gold films with a thickness of 10 nm before observation. Fiber diameters were measured using Image J 1.40 G software (http://rsb.info.nih.gov/ij/down-load.html). At least 100 nanofibers from different SEM images for each sample were randomly selected and analyzed. TEM was performed using a Hitachi H-800 transmission electron microscope (Tokyo, Japan) with a voltage of 200 kV. The suspension of LAP nanodisks dispersed in THF–DMF was dropped onto a carbon-coated copper grid, and air dried before measurement. For the nanofiber samples, the LAP-doped PLGA nanofibers were directly electrospun onto the carbon-coated copper grid and vacuum dried before TEM imaging. TGA was performed on a TG209F1 system (NETZSCH Instruments Co., Ltd., Germany). Fiber samples were heated from room temperature to 600 °C with a heating rate of 20 °C $min^{-1}$ under air atmosphere. To determine the porosity of the fibrous samples, three small strips (20 × 20 $mm^2$) were cut from the center of the nanofibrous mats, and the porosity of the fibrous mats was calculated using the following equations:[16,49]

$$\rho_a(\text{g cm}^{-3}) = \frac{m(\text{g})}{d(\text{cm}) \times s(\text{cm}^2)} \quad (1)$$

$$p = \left(1 - \frac{\rho_a(\text{g cm}^{-3})}{\rho_b(\text{g cm}^{-3})}\right) \times 100\% \quad (2)$$

where $\rho_a$ and $\rho_b$ stand for apparent density of nanofibers and bulk density of PLGA or LAP-doped PLGA nanofibers, respectively, $p$, $m$, $d$, and $s$ stand for porosity, mass, thickness (measured with a micrometer), and area of the strip, respectively. Note that the bulk density of LAP-doped PLGA nanofibers was calculated based on the composition of PLGA (1.25 g $cm^{-3}$)[16] and LAP (2.60 g $cm^{-3}$).[50] The mechanical properties of the electrospun fibrous mats were examined using a materials testing machine (H5K-S, Hounsfield, UK) with an elongation speed of 10 mm $min^{-1}$ at 20 °C and a relative humidity of 63%. Before measurements, three pieces of rectangular nanofibrous mats were cut into a dimension of 10 mm × 50 mm. Stress and strain were calculated through the following equations:[13,16]

$$\sigma(\text{MPa}) = \frac{P(N)}{w(\text{mm}) \times d(\text{mm})} \quad (3)$$

$$\varepsilon = \frac{l}{l_0} \times 100\% \quad (4)$$

where $\sigma$, $\varepsilon$, $P$, $w$, $d$, $l$, and $l_0$ stand for stress, strain, load, mat width, mat length, extension length, and gauge length, respectively. The breaking strength, failure strain and Young's modulus were obtained from the strain–stress curves. The surface hydrophilicity of the PLGA and LAP-doped PLGA fibrous mat was evaluated *via* a water contact angle test. A pendant droplet of distilled water with a drop size of 1 μL was dropped onto the surface of each sample at the randomly selected area for three times at ambient temperature and humidity. The contact angle was measured using a contact angle goniometer (DSA-30, Kruss, Germany) when the droplet was stable.

### Protein adsorption onto LAP-doped PLGA nanofibers

The protein adsorption test was carried out according to our previous study.[21] Briefly, cover slips, and PLGA or PLGA–LAP nanofibers electrospun onto cover slips were fixed in a 24-well tissue culture plate (TCP). Before measurements, each sample in triplicate was sterilized by exposure to 75% ethanol for 1 h and then soaked with PBS solution for additional 2 h. After that, TCPs, cover slips, PLGA, and LAP-doped PLGA nanofibers were incubated with 1 mL FBS (10%) solution for 24 h at 37 °C. The concentrations of FBS before and after adsorption were quantified using a Lambda 25 UV-Vis spectrophotometer (Perkin Elmer, USA) at 280 nm with the aid of the FBS calibration curve at the same wavelength.

### Cytocompatibility evaluation

The cytocompatibility of the PLGA or LAP-doped PLGA nanofibers was assessed *via* MTT assay and cell morphology observation. In brief, cover slips, and PLGA or PLGA–LAP nanofibers on cover slips were fixed in a 24-well TCP with stainless rings and sterilized by exposure to 75% alcohol solution for 2 h. After that, all samples were washed 3 times with PBS solution and soaked in DMEM overnight before cell seeding. Then, L929 or PIECs were seeded at a density of 1.5 × $10^4$ cells per well for cell attachment and proliferation assay and at a density of 2 × $10^4$ cells per well for SEM morphology observation, respectively. TCP and cover slips without nanofibers were used as controls.

The viability of L929 and PIECs was quantitatively evaluated using MTT assay after cell seeding for 1, 4, and 8 h for cell attachment assay and 1, 3, and 7 days for cell proliferation assay, respectively. At each time point, MTT solution (40 μL) was added to each well, followed by incubating for another 4 h at 37 °C. After that, DMSO (400 μL) was added to each well with

shaking at 37 °C for 15 min to dissolve the purple MTT formazan crystal. Then, the dissolved formazan solution (100 μL) of each sample was transferred into individual wells of a 96-well plate and the optical density (OD) value at 570 nm was measured by a microplate reader (MK3, Thermo, USA). The mean and standard deviation from the triplicate wells for each sample were reported.

The cell morphology was observed by SEM (JEOL JSM-5600LV, Japan) with an accelerating voltage of 10 kV. In brief, cell samples at different time points were rinsed 3 times with PBS solution to remove non-adherent cells. Then, each sample was fixed with 2.5 wt% glutaraldehyde at 4 °C for 2 h, followed by dehydrating through a series of gradient ethanol solutions of 30, 50, 70, 80, 90, 95, and 100%, and air dried overnight. Before SEM observation, samples were sputter coated with a 10 nm thick gold film.

### Hemocompatibility test

The hemocompatibility of the formed PLGA or PLGA–LAP nanofibers was examined by both hemolysis and anticoagulant assays. For hemolysis assay, the human red blood cells (HRBCs) were obtained by removing the serum *via* centrifugation and washing with PBS 5 times according to the literature.[51–53] After that, the HRBCs were 10 times diluted with PBS. Then, 2 mL of the diluted HRBCs suspension was transferred to a 5 mL sample vial containing 1 mg of PLGA, PLGA–1% LAP, PLGA–3% LAP, and PLGA–5% LAP fibrous mats, respectively. Another two sample vials containing 0.4 mL of the diluted HRBCs and 1.6 mL of water or PBS solution were set as a positive and negative control, respectively. The above mixtures were then incubated at 37 °C for 2 h, followed by centrifugation (10 000 rpm, 1 min) and the absorbance of the supernatants related to hemoglobin was recorded with a Lambda 25 UV-Vis spectrophotometer (Perkin Elmer, USA) at 541 nm. The hemolytic percentage (HP) was calculated using the following equation,[51]

$$\mathrm{HP}(\%) = \frac{(D_t - D_{nc})}{(D_{pc} - D_{nc})} \times 100\% \quad (5)$$

where $D_t$ is the absorbance of the test samples; $D_{pc}$ and $D_{nc}$ are the absorbances of the positive and negative control, respectively.

The anticoagulant property of the PLGA or LAP-doped PLGA nanofibers was evaluated by the kinetic clotting time method according to the procedures reported in the literature.[51,54] The as-prepared nanofibers were cut into small pieces in dimensions of 20 mm × 20 mm in three parallels and were put into individual wells of 12-well TCP. Cover slips without nanofibers were used as a control. Then, a 20 μL of fresh human blood was dropped onto the surface of the fiber samples and the cover slips, followed by addition of 10 μL of $CaCl_2$ (0.2 mol $L^{-1}$) solution to each blood drop and incubated at 37 °C for a predetermined period of time (5, 10, 20, 40, and 60 min, respectively). After that, 5 mL distilled water was put into each well carefully and incubated at 37 °C for 5 min. The concentration of hemoglobin in water was measured by monitoring the absorbance at 541 nm using a Lambda 25 UV-Vis spectrophotometer (Perkin Elmer, USA).

### hMSC culture and seeding

Small pieces of human bone marrow were harvested from patients and kept in sterilized tubes at 4 °C in α-MEM supplemented with 10% FBS and 1% antibiotic–antimycotic solution (Gibco) no longer than 20 h. After that, primary cell cultures were established by carefully shaking the tubes containing the bone marrow fragments to generate a cell suspension, which was then distributed by cell culture dishes (Corning, USA). The culture medium was changed after 24 h to remove non-adherent hematopoietic cells and, after, twice a week until 80% confluence was reached. The cells were then twice passaged and frozen in liquid nitrogen. α-MEM supplemented with 10% FBS and 1% antibiotic–antimycotic solution was used throughout this process. For the following experiments, α-MEM containing 1% ascorbic acid solution (5 mg $mL^{-1}$ in PBS) and 1% β-GP solution (1 M in PBS) was used. Before cell seeding, PLGA and LAP-doped (5% LAP relative to PLGA) nanofibers were sterilized as mentioned above. TCPs without materials were set as a control. Then, hMSCs (passage 3) were seeded at a density of $2 \times 10^4$ cells per well (24-well plates, Corning, USA) with 1 mL growth α-MEM or 1 mL 'osteogenic medium' (growth medium containing $10^{-7}$ M DEX) per well. For all cells, the medium was replaced every 3 days and incubated at 37 °C in a humidified atmosphere with 5% $CO_2$.

### Metabolic activity of the hMSCs

The metabolic activity of hMSCs cultured onto nanofiber scaffolds was evaluated using the resazurin reduction assay according to the literature.[55] At each time point (1, 7, 14, and 21 days, respectively), medium was replaced with 900 μL growth medium or osteogenic medium and 100 μL resazurin solution (0.1 mg $mL^{-1}$ in PBS). Then the plate was incubated for 4 h, and the fluorescence intensity ($\lambda_{ex}$ = 530 nm and $\lambda_{em}$ = 590 nm) was measured by a Victor$^3$ 1420 multilabel plate reader (Perkin Elmer, USA). The mean and standard deviation for the triplicate wells for each sample were reported.

### Alkaline phosphatase activity and DNA content

After 14 and 21 days of culture, hMSCs cultured in a 24-well plate were rinsed 3 times with PBS. Then, 200 μL Reporter Lysis Buffer was added to each well and the cell lysis was done according to the manufacturer's instruction. The cell lysates were stored at −20 °C before analysis.

Alkaline phosphatase (ALP) activity was assessed by the hydrolysis of *p*-nitrophenyl phosphate as the substrate. Briefly, 20 μL of the cell lysates was mixed with 200 μL of ALP substrate and incubated for 1 h at 37 °C in the dark. Then, 10 μL of 0.02 M NaOH was added to each well to stop the hydrolysis reaction. 220 μL of ALP substrate mixed with 10 μL of 0.02 M NaOH was added into 3 individual wells and used as a blank control. The absorbance was read at 405 nm and the ALP content was calculated from a standard calibration curve.

The Picogreen DNA quantification kit was used to quantify the DNA content of each cell sample. Briefly, 20 μL cell lysates was transferred to a clean 96-well and then diluted with 80 μL Tris-EDTA (TE) buffer. Then, a 100 μL Picogreen working reagent was added to each well and incubated at room

 

temperature for 5 min. Then, the fluorescence intensity ($\lambda_{ex} = 485$ nm and $\lambda_{em} = 538$ nm) was monitored by a Victor$^3$ 1420 multi-label plate reader (Perkin Elmer, USA). The DNA content was calculated from a standard calibration curve.

### Osteocalcin secretion

The osteocalcin secretion on day 14 and day 21 was measured using an intact human osteocalcin EIA kit (Biomedical Technologies Inc., USA). One day before analysis, the medium was replaced with fresh medium (growth α-MEM without FBS or osteogenic medium without FBS). After 24 h of cell culture, the medium was transferred to a clean Eppendorf tube and the osteocalcin content was analyzed using the intact human osteocalcin EIA kit according to the manufacturer's instructions.

### Calcium content assay

The QuantiChrom Calcium Assay Kit was used to determine the calcium content according to the manufacturer's instructions. Briefly, 0.1 mL of cell lysates was mixed with 0.1 mL of 2 M HCl to dissolve the calcium deposits for 5 min. After that, 20 μL aliquot of the supernatant was mixed with 180 μL of working reagent of the kit and incubated at room temperature for 3 min, and the absorbance was read at 590 nm using a microplate reader (MK3, Thermo, USA). The $Ca^{2+}$ concentration was calculated from a standard calibration curve.

### Histochemical assay

Before histochemical assay, cells were first fixed with 3.7% formaldehyde in PBS solution for 2 h at 4 °C and then rinsed with water for 3 times to remove all traces of formaldehyde. For the ALP staining, the fixed cells was covered with a working solution which was made by mixing sodium α-naphthyl phosphate (2 mg $mL^{-1}$) and fast blue RR salt (2 mg $mL^{-1}$) solutions, both prepared in 0.1 M Tris buffer (pH = 10). The working solution was filtered through a 0.45 μm filter before use. After incubating for 45 min at room temperature, the cells were washed twice with water before observation using a Nikon Eclipse TE2000-E inverted microscope (Japan). For the von Kossa staining, the fixed cells were first treated with 2.5% silver nitrate solution and exposed under ultra-violet light for 60 min. After rinsing with water, the cells were treated with 5% sodium thiosulfate solution for 3 min, followed by rinsing with water thoroughly. Finally, the cell samples were taken out from the culture plates and photographed using a Cannon digital camera (PowerShot SX110 IS).

### Statistical analysis

One way ANOVA statistical analysis was performed to compare the protein adsorption onto different substrates, the cytocompatibility of cells cultured onto different materials, hemocompatibility of different nanofiber samples, and metabolic activity, ALP activity, osteocalcin secretion capability and calcium content of hMSCs cultured onto different substrates. The $p$ value of 0.05 was selected as the significance level, and the data were indicated with (*) for $p < 0.05$, (**) for $p < 0.01$, and (***) for $p < 0.001$, respectively. Each experiment was done in triplicate ($n = 3$).

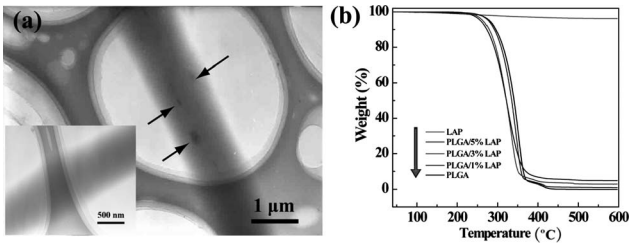


**Fig. 1** (a) TEM micrographs of PLGA (inset) and 5 wt% LAP-doped PLGA nanofibers with arrows indicating the doped LAP nanodisks. (b) TGA profiles of PLGA and LAP-doped PLGA nanofibers.

## Results and discussion

### Characterization of PLGA and LAP-doped PLGA nanofibers

Similar to our previous work related to the incorporation of halloysite nanotubes within PLGA nanofibers,[16] we were able to incorporate LAP nanodisks within PLGA nanofibers. The LAP nanodisks were able to be well dispersed within the 25% PLGA solution in a solvent mixture of THF–DMF (v/v = 3 : 1)

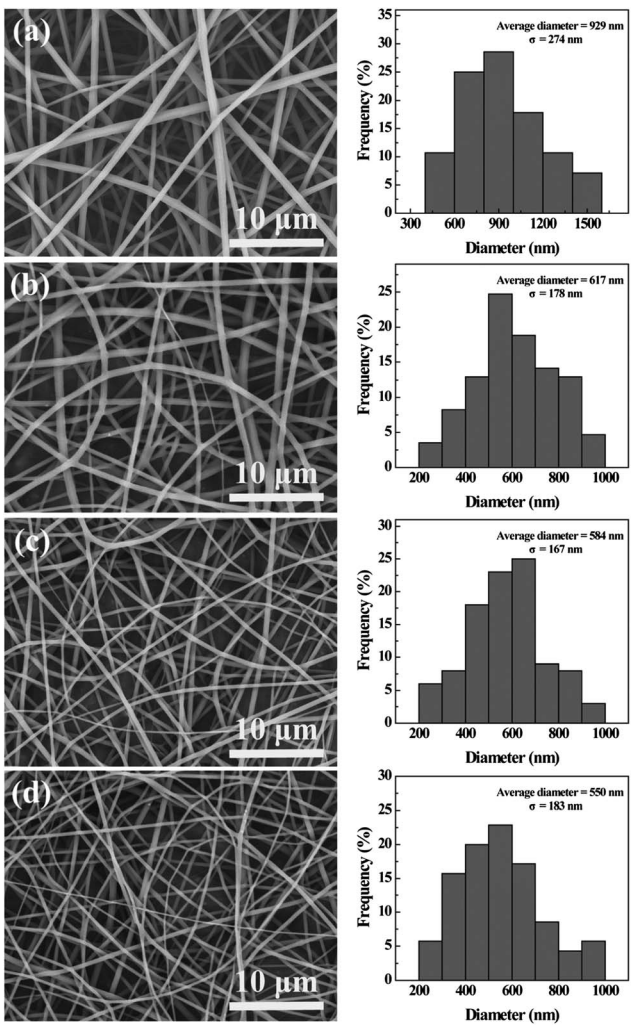


**Fig. 2** SEM micrographs and diameter distribution histograms of (a) PLGA and LAP-doped ((b) 1%, (c) 3%, and (d) 5% LAP relative to PLGA, respectively) PLGA nanofibers.

(Fig. S1a, ESI†). TEM images of the LAP nanodisks show that the LAP nanodisks have a mean diameter of 19.1 ± 2.3 nm with quite a uniform size distribution (Fig. S1b, ESI†). After incorporation within PLGA nanofibers, the LAP nanodisks appeared to form flake-shaped aggregates primarily due to the solvent drying process during the electrospinning (Fig. 1a). In contrast, pure PLGA nanofibers did not have such aggregated structures that are related to the existence of LAP (Fig. 1a, inset). The existence of the doped LAP in the nanofibers was further confirmed by TGA (Fig. 1b). Obviously, the polymer was burned out at a high temperature above 400 °C and LAP residues were left out. The mass residuals of PLGA–1% LAP, PLGA–3% LAP, and PLGA–5% LAP nanofibers at 600 °C were determined to be 0.97%, 2.76%, and 4.78%, respectively, in agreement with the initial molar feeding percentages.

The morphology of the electrospun PLGA and LAP-doped PLGA nanofibers was observed by SEM (Fig. 2). Smooth and uniform nanofibers were able to be prepared in all the cases and the 3-dimensional morphology of PLGA nanofibers did not significantly change after the LAP incorporation. However, when compared with the pure PLGA nanofibers, the diameter of PLGA–1% LAP (617 ± 178 nm, Fig. 2b), PLGA–3% LAP (584 ± 167 nm, Fig. 2c), and PLGA–5% LAP (550 ± 183 nm, Fig. 2d) nanofibers decreased dramatically with the LAP doping level. The fiber diameter change should be due to the change of the electrospinning solution properties.[28] The decreased fiber diameter with the LAP doping level is likely ascribed to the increase of the solution conductivity since LAP is inherently ionic.[56]

The decrease of the nanofiber diameter with the LAP doping level led to a variation in the porosity of the nanofibrous mat. As shown in Table 1, it appears that the porosity of the PLGA fibrous mat (72.1%) decreases to about 64–65% after doping with 1–5% LAP (relative to PLGA), which is likely due to the decreased fiber diameter after LAP doping, causing much denser fiber arrangement.

Besides the change of the PLGA nanofiber diameter and porosity after LAP doping, the influence of the LAP doping on the mechanical durability of the PLGA nanofibrous mat was also investigated. The representative strain–stress curves and the images of the PLGA nanofibers with or without LAP doping are shown in Fig. 3, and the mechanical parameters are listed in Table S1 (ESI†). It is clear that the breaking strength and Young's modulus increase after the LAP doping, in agreement with literature data.[16] The increased breaking strength and Young's modulus may be due to the efficient load transfer from the PLGA matrix to the doped LAP nanodisks. However, the failure strain decreased after the loading of LAP, primarily due to the increased brittleness of the fibers with the LAP doping level.

**Table 1** Apparent density, bulk density and porosity of PLGA and LAP-doped PLGA nanofibers (all data are given as mean ± SD, $n = 3$)

| Sample | Apparent density (g cm$^{-3}$) | Bulk density[a] (g cm$^{-3}$) | Porosity (%) | Water contact angle (°) |
|---|---|---|---|---|
| PLGA | 0.35 ± 0.037 | 1.25 | 72.1 ± 0.03 | 128.7 ± 3.6 |
| PLGA–1% LAP | 0.44 ± 0.036 | 1.26 | 65.4 ± 0.03 | 120.2 ± 0.8 |
| PLGA–3% LAP | 0.45 ± 0.028 | 1.27 | 64.4 ± 0.02 | 112.6 ± 1.1 |
| PLGA–5% LAP | 0.46 ± 0.035 | 1.28 | 64.1 ± 0.03 | 113.2 ± 3.4 |

[a] Bulk density can be calculated from the following equation: $\frac{1}{\rho} = \frac{\omega_1}{\rho_1} + \frac{\omega_2}{\rho_2}$, where $\rho$ stands for the bulk density, $\omega_1$ and $\omega_2$ stand for the weight ratio of PLGA and LAP in the nanofibers, respectively. $\rho_1$ and $\rho_2$ represent the bulk density of PLGA (1.25 g cm$^{-3}$)[16] and LAP (2.60 g cm$^{-3}$),[50] respectively.

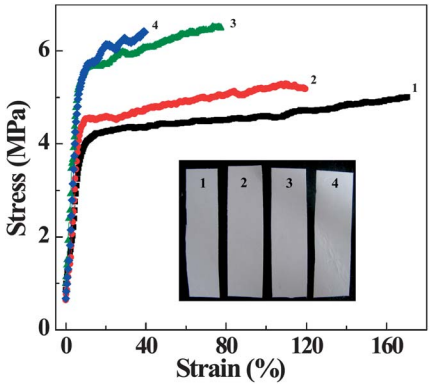


**Fig. 3** Strain–stress curves of PLGA (1), PLGA–1% LAP (2), PLGA–3% LAP (3), and PLGA–5% LAP (4) nanofibers. The inset shows the representative image of PLGA (1), PLGA–1% LAP (2), PLGA–3% LAP (3), and PLGA–5% LAP (4) nanofibrous mats, respectively.

The surface hydrophilicity of nanofibers is one of the key parameters affecting their interactions with cells. We next explored the influence of LAP doping on the surface hydrophilicity of the PLGA nanofibers. Water contact angle tests show that the contact angle of PLGA nanofibers (128.7 ± 3.6°) decreases to be 120.2 ± 0.8°, 112.6 ± 1.1°, and 113.2 ± 3.4° after doping with 1%, 3%, and 5% LAP, respectively (Fig. S2, ESI† and Table 1). This suggests that the hydrophilicity of the PLGA nanofibrous mat slightly increases with the amount of the incorporated LAP. Since the porosity of LAP-doped PLGA nanofibers remains approximately similar (Table 1), the increase of hydrophilicity of the mats with the doping level of LAP is likely due to the hydrophilic nature of the LAP material. The increased hydrophilicity of PLGA nanofibers after LAP doping may facilitate the infiltration of hydrophilic nutrient substances and tune the cell response on the mat surface.

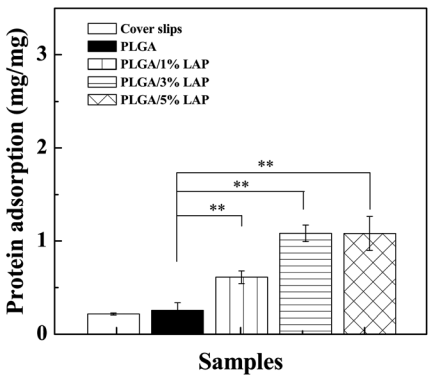


**Fig. 4** The adsorption of protein (mg protein per mg substrate) onto the cover slip, PLGA, and LAP-doped PLGA nanofibers (mean ± SD, $n = 3$).

 

### Protein adsorption onto PLGA and LAP-doped PLGA nanofibers

An ideal scaffolding material should allow more protein adsorption onto its surface, and therefore providing better biocompatibility for cell growth and migration.[21] With the increased surface hydrophilicity after LAP doping, the protein adsorption onto LAP-doped PLGA nanofibers should be different. We then explored the impact of LAP doping on the protein adsorption behavior of PLGA nanofibers (Fig. 4). It can be seen that significantly more protein was adsorbed onto the surface of PLGA–1% LAP, PLGA–3% LAP, and PLGA–5% LAP nanofibers than onto the cover slip (for all LAP-doped PLGA nanofibers, $p < 0.01$). Moreover, the LAP-doped PLGA scaffolds could absorb more protein than the LAP-free PLGA nanofibers ($p < 0.01$ for all LAP-doped PLGA nanofibers). The increased protein adsorption onto LAP-doped PLGA nanofibers may be caused by the additional adsorption of protein onto the doped LAP in the nanofibers. In addition, the porous fibrous structure in individual nanofibers is likely to be expanded due to the incorporation of LAP, which is favorable for protein adsorption. This result is in agreement with our previous data related to halloysite nanotube-incorporated PLGA nanofibers.[21] This clearly indicates that the incorporation of LAP facilitates more protein adsorption, therefore likely inducing enhanced cellular response.

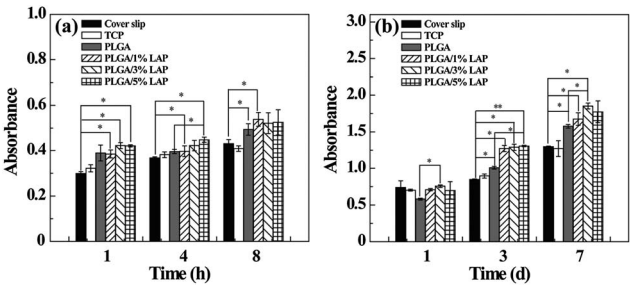


**Fig. 5** Attachment (a) and proliferation (b) levels of L929 cells seeded onto the cover slips, TCP, electrospun PLGA and LAP-doped PLGA nanofibers (mean ± SD, $n = 3$).

### Cytocompatibility assay of PLGA and LAP-doped PLGA nanofibers

The cytocompatibility of PLGA and LAP-doped PLGA nanofibers was studied by evaluating the metabolic activity of L929 and PIECs cultured onto the nanofiber scaffolds using the MTT assay (Fig. 5 and S3, ESI†). The OD value is in direct proportion to the cell metabolic activity and, thus, to the number of viable cells. The adhesion and proliferation levels of L929 and PIECs cultured onto the PLGA and LAP-doped PLGA nanofibers are obviously better than those of the cells cultured onto the cover slips at different time points, and a significant difference can be found between the cover slip and nanofibers at different time points. It is worth noting that both the adhesion and proliferation levels of L929 and PIECs cultured onto LAP-doped PLGA are better than those of cells cultured onto LAP-free PLGA nanofibers ($p < 0.05$ and $p < 0.01$, respectively, as shown in Fig. 5 and S3†), which may be attributed to the increased surface hydrophilicity and the enhanced protein adsorption of the LAP-doped PLGA nanofibers.

The morphology of L929 and PIECs seeded onto the LAP-doped PLGA nanofibrous mats for 8 h and 3 days was observed by SEM (Fig. 6 and S4 in the ESI†). Both L929 and PIECs could be better adhered and proliferated onto PLGA and LAP-doped PLGA nanofibers, qualitatively corroborating the MTT assay data.

### Hemocompatibility assay of PLGA and LAP-doped PLGA nanofibers

Hemocompatibility has been considered as one of the key issues, especially when the designed fibrous scaffold materials need to contact blood.[51] Therefore, besides the required cytocompatibility, another major concern of an ideal material to be used in tissue engineering is its hemocompatibility. The hemocompatibility of LAP-doped PLGA nanofibers was evaluated *via* hemolysis and anticoagulant assay *in vitro*, respectively (Fig. 7). We showed that after exposure of PLGA and LAP-doped PLGA nanofibers to the HRBCs, no visible hemolysis phenomenon was observed, similar to the HRBCs exposed to PBS solution utilized

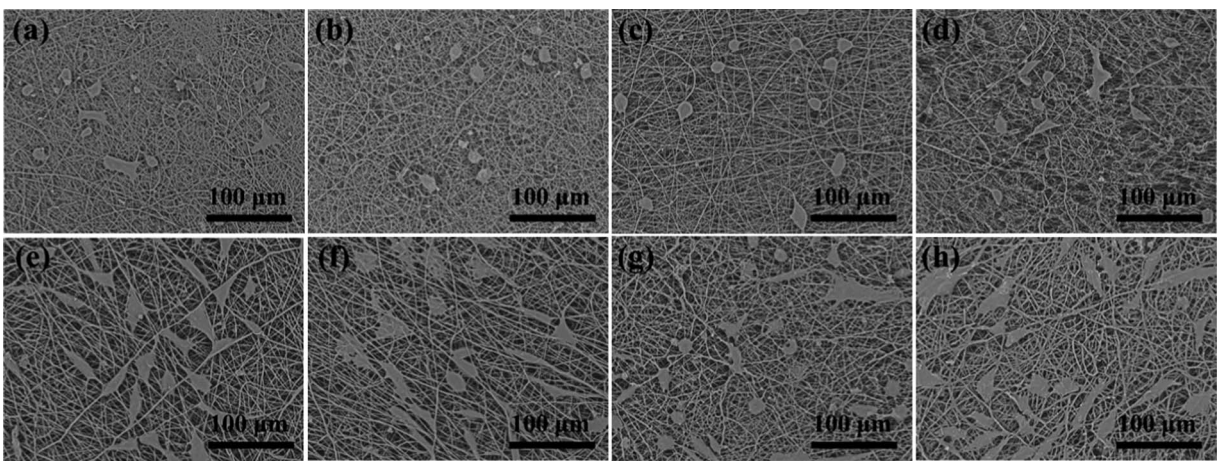


**Fig. 6** SEM micrographs of L929 cells attached (a–d) and proliferated (e–h) onto the (a and e) PLGA nanofibers, and LAP-doped ((b and f) 1%, (c and g) 3%, and (d and h) 5% LAP relative to PLGA, respectively) PLGA nanofibers after 8 h (a–d) and 3 days (e–h) of culture, respectively.

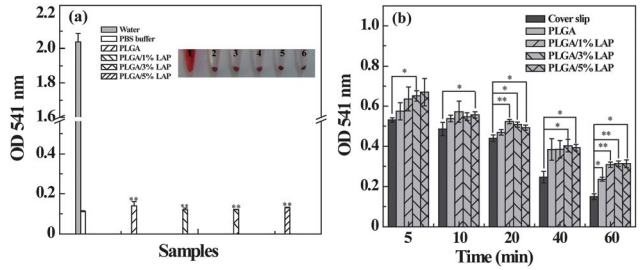


**Fig. 7** (a) Hemolytic assay of HRBCs after treatment with distilled water, PBS solution, PLGA and LAP-doped PLGA nanofibers for 2 h. The inset shows the photograph of HRBC suspensions exposed to (1) distilled water, (2) PBS solution, (3) PLGA nanofibers, and LAP-doped ((4) 1%, (5) 3%, and (6) 5% LAP relative to PLGA, respectively) PLGA nanofibers for 2 h, followed by centrifugation. (b) Dynamic clotting behavior of PLGA and LAP-doped PLGA nanofibers as a function of time (mean ± SD, $n = 3$).

as a negative control. In contrast, after exposure of the HRBCs to water, a positive control, the HRBCs were totally damaged (inset of Fig. 7a). The hemolytic effects of each sample were further quantified by recording the absorbance of the supernatant at 541 nm which is in direct proportion to the hemoglobin concentration using UV-Vis spectroscopy. As shown in Fig. 7a, a significant difference ($p < 0.01$) in the OD value can be found between the positive control group (HRBCs exposed to distilled water) and the experimental groups having hemolysis percentages all lower than 5% (1.5 ± 0.9%, 0.7 ± 0.4%, 0.5 ± 0.1%, and 1.2 ± 0.2% for PLGA, PLGA–1% LAP, PLGA–3% LAP, and PLGA–5% LAP nanofibers, respectively). It indicates that PLGA and LAP-doped PLGA nanofibers do not show any appreciable hemolytic effect. The blood clotting behavior of PLGA and LAP-doped PLGA nanofibers was also studied (Fig. 7b). A higher OD value representing a higher hemoglobin concentration suggests that the clotting behavior is less obvious. We show that the control group has a significantly higher OD value associated with the higher clotting phenomenon at each time point ($p < 0.05$ and $p < 0.01$, respectively), implying that PLGA and LAP-doped PLGA nanofibers possess better anticoagulation capacity than the cover slip. Our studies show that although the incorporation of LAP improves the hydrophilicity and protein adsorption behavior of PLGA nanofibers, the anticoagulation property of LAP-doped PLGA nanofibers does not significantly change when compared with pure PLGA nanofibers. Taken together with both the hemolysis and anticoagulation assay data, we can conclude that the LAP-doped PLGA nanofibers possess good hemocompatibility, which is essential for their applications in tissue engineering.

### Metabolic activity of hMSCs cultured onto LAP-doped PLGA nanofibers

The good cytocompatibility and hemocompatibility of LAP-doped PLGA nanofibers lead us to use them as a scaffold material for osteogenic differentiation of hMSCs. In our study, we selected PLGA–5% LAP nanofibers as a model scaffold for stem cell differentiation studies. We first analyzed the metabolic activity of the hMSCs cultured onto LAP-doped PLGA nanofibers. Fig. 8 shows resazurin reduction assay data of hMSCs at

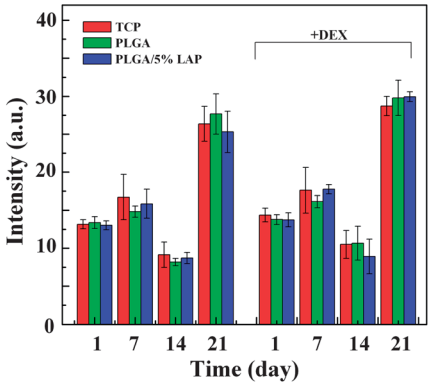


**Fig. 8** Metabolic activity assay of hMSCs cultured onto TCP, PLGA and PLGA–5% LAP nanofibers in growth medium and osteogenic medium at different culture times (mean ± SD, $n = 3$).

different time points in both growth medium and osteogenic medium. Apparently, during the first 14 days, the metabolic activity of hMSCs decreased in both growth and osteogenic medium, which can be ascribed to a long lag phase and partial cell death. After that, hMSCs experience an exponential phase and the metabolic activity is enhanced rapidly during day 14 to day 21. This is typical for the growth of hMSCs when attached to an exogenous matrix.[57] Besides, metabolic activity of hMSCs cultured onto both PLGA and PLGA–LAP nanofibers does not show any significant difference when compared to that onto the TCP control, implying that hMSCs are able to proliferate well on both PLGA and PLGA–LAP nanofiber scaffolds.

### ALP activity of hMSCs cultured onto LAP-doped PLGA nanofibers

ALP enzyme is usually highly active in osteoblasts involved in the early initiation of mineralization of newly formed bone tissue and has been used as an important marker of osteogenesis.[58] The ALP activity of hMSCs was measured on day 14 and day 21 (more prominent values are expected to be detected at these time points), and the results (normalized for the total DNA content)

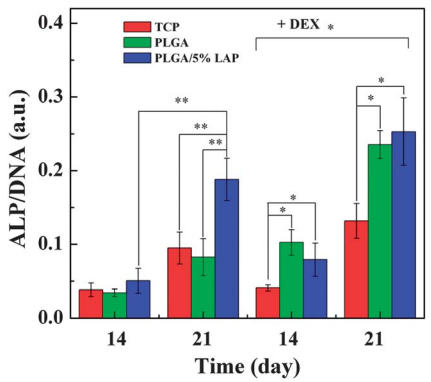


**Fig. 9** ALP activity (normalized for the DNA content, nmol of transformed substrate per unit of time and per mass of DNA) of hMSCs cultured onto TCP, PLGA and PLGA–5% LAP nanofibers in growth medium and osteogenic medium at different culture times (mean ± SD, $n = 3$).

 

are shown in Fig. 9. It is clear that, from day 14 to day 21, hMSCs cultured onto TCP and PLGA nanofibers in growth medium show a moderate increase in the ALP activity, while hMSCs cultured onto PLGA–5% LAP nanofibers show a significantly higher ALP activity ($p < 0.01$). Besides, on day 21, hMSCs cultured onto PLGA–5% LAP nanofibers also showed a significantly higher ALP activity ($p < 0.01$) than those cultured onto PLGA nanofibers and the TCP control in growth medium. These results suggest that PLGA–5% LAP nanofibers can induce osteogenic differentiation of hMSCs in growth medium without any inducing factors. Literature data have shown that a calcium magnesium silicate bioceramic (akermanite) is able to enhance bone marrow-derived stem cell proliferation and differentiation due to the role played by ionic Si and Mg of the akermanite.[59] It is reasonable to deduce that as an Si- and Mg-rich nanoclay material with good biodegradability, the incorporated LAP should play an important role in the regulation of the osteogenic differentiation of the hMSCs.

The ALP activity of hMSCs cultured in osteogenic medium on day 14 and day 21 was also studied in comparison with that in growth medium. As shown in Fig. 9, a significant difference ($p < 0.05$) in ALP activity of hMSCs cultured onto nanofibers and onto TCP can be observed between day 14 and day 21. The ALP activity of hMSCs cultured onto each material on day 21 is significantly higher than that on day 14. Both pure PLGA and PLGA–5% LAP nanofiber groups have much higher ALP activity than the TCP control ($p < 0.05$), suggesting that the ECM mimicking property of nanofibrous scaffolds are able to promote the osteoblast differentiation of hMSCs.[60] Clearly, in osteogenic medium, the LAP-doped PLGA nanofibers did not show a significant difference in ALP activity when compared with pure PLGA nanofibers, indicating that the osteogenic differentiation of hMSCs can occur in both cases due to the strong osteogenic inducing effect of the added DEX.

To further qualitatively confirm the osteoblastic differentiation of hMSCs cultured onto LAP-doped PLGA nanofibers, histochemical assay of ALP activity was performed by staining the hMSCs with a solution mixture of sodium α-naphthyl phosphate and fast blue RR salt. The ALP staining results are shown in Fig. S5 (ESI†). Light and dark brown parts represent low and high ALP activity positive areas, respectively. The microscopic images illustrate the osteoblast differentiation of hMSCs in PLGA–5% LAP nanofibers, similar to those cultured onto pure PLGA nanofibers and PLGA–5% LAP nanofibers in osteogenic medium. This further confirms that the LAP-doped PLGA nanofibers are able to induce the osteoblast differentiation of hMSCs even in growth medium without DEX.

### Osteocalcin secretion

Osteocalcin is an important marker for late-stage osteoblast differentiation. The extracellular osteocalcin production content of hMSCs cultured onto different substrates (TCPs, PLGA nanofibers, and LAP-doped PLGA nanofibers) was also assayed on days 14 and 21 (more prominent values are expected to be detected at these time points) and the results are shown in Fig. 10. It can be clearly seen that on day 14, hMSCs cultured in both growth medium and osteogenic medium show a very low osteocalcin production. On day 21, the osteocalcin production

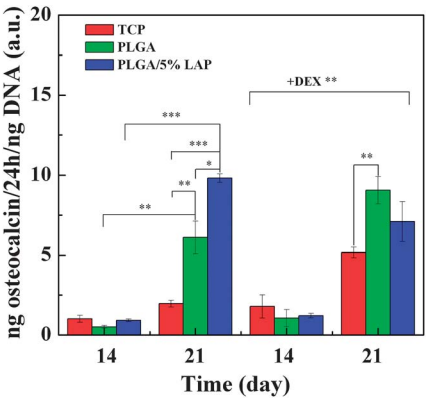


**Fig. 10** Osteocalcin secretion of hMSCs cultured onto TCP, PLGA and PLGA–5% LAP nanofibers in growth medium and osteogenic medium at different culture times (mean ± SD, $n = 3$).

content of hMSCs cultured in both growth medium and osteogenic medium was higher than that on day 14, revealing the progression of osteogenic differentiation. In growth medium, hMSCs cultured onto either PLGA or LAP-doped PLGA nanofibers produced significantly higher osteocalcin than that of hMSCs cultured onto the TCP control ($p < 0.001$ and $p < 0.01$ for PLGA–5% LAP nanofibers and pure PLGA nanofibers, respectively) on day 21. In addition, the PLGA–5% LAP group had much high osteocalcin production than the pure PLGA nanofiber group ($p < 0.05$), further confirming the role played by the incorporated LAP within PLGA nanofibers. It should be noted that for the pure PLGA nanofiber group, the more significant osteocalcin production than the TCP control ($p < 0.01$) may be related to the nanofibrous structure, which may enable osteogenic differentiation of hMSCs by forcing the cells into an elongated, highly branched, osteogenic morphology, as demonstrated by Simon and coworkers.[60] In osteogenic medium, the TCP control had much higher osteocalcin secretion than the same control in growth medium without DEX, indicating that the added DEX is able to induce the osteogenesis of hMSCs. Both the pure PLGA and PLGA–5% LAP nanofiber groups had much more osteocalcin secretion than the TCP control, similar to the ALP activity assay data. Overall, the assay of the late-stage marker osteocalcin proves that the LAP doped within PLGA nanofibers is soundly beneficial for osteogenic differentiation of hMSCs in the absence of osteogenic supplements.

### Calcium content assay

The calcium content after 14 and 21 days of culture was quantified to further confirm the osteogenic differentiation of hMSCs cultured onto different nanofiber scaffolds. As shown in Fig. 11, hMSCs cultured with osteogenic medium have relatively higher calcium content than that of the hMSCs cultured in growth medium without DEX under similar conditions (fiber substrate and time point). The hMSCs cultured on day 21 have a significantly higher calcium content than those cultured on day 14, which is due to the inducing activity of the added DEX. Importantly, hMSCs cultured onto PLGA–5% LAP nanofibers in growth medium without DEX show a significantly higher calcium content than those cultured onto LAP-free PLGA nanofibers (day 14, $p < 0.01$ and day 21, $p < 0.05$). This further

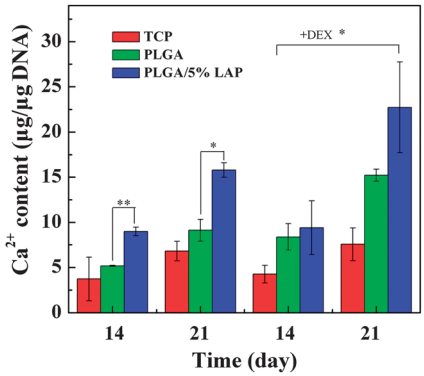


**Fig. 11** Calcium content of hMSCs cultured onto TCP, PLGA and PLGA–5% LAP nanofibers in growth medium and osteogenic medium at different culture times (mean ± SD, $n = 3$).

confirmed that PLGA–5% LAP nanofibers enabled the osteogenic differentiation of hMSCs in growth medium without any inducing factors.

### von Kossa staining

The fixed hMSCs were also stained to qualitatively confirm the presence of calcium phosphate crystals by von Kossa staining. As shown in Fig. S6 (ESI†), hMSCs cultured onto both PLGA and PLGA–5% LAP nanofibers were all stained in the dark in the presence of osteogenic medium, indicating the production of calcium phosphate crystals. For hMSCs cultured with growth medium without any inducing factors, only PLGA–5% LAP nanofibers enabled the dark staining of the hMSCs, suggesting a similar osteogenic differentiation of the hMSCs. The formation of calcium phosphate crystals is the late-stage marker of osteogenic differentiation of hMSCs.[61] Therefore, the von-Kossa staining data qualitatively confirmed that the osteogenic differentiation of hMSCs could be enabled by PLGA–5% LAP nanofibers without any inducing factors.

## Conclusions

In summary, electrospun LAP-doped PLGA nanofibers were prepared and used as scaffold materials for tissue engineering applications. Our results show that the LAP nanodisks can be directly electrospun onto the PLGA nanofibers without changing the uniform PLGA nanofiber morphology. However, the incorporation of LAP leads to the decrease of the diameter and porosity, and the increase of the surface hydrophilicity, protein adsorption capacity, and mechanical durability of the PLGA nanofibers. MTT assays and SEM studies show that the incorporated LAP within PLGA nanofibers is helpful to facilitate better cell adhesion and proliferation of L929 and PIECs when compared to pure PLGA nanofibers. Importantly, the LAP-doped PLGA nanofibers were able to be used as a scaffold material for osteogenic differentiation of hMSCs in both growth medium and osteogenic medium. Our results show that the LAP-doped PLGA nanofibers are able to induce the osteoblast differentiation of hMSCs in growth medium without any inducing factors, which is primarily due to the significant role played by LAP, an Si- and Mg-rich nanoclay material with good biodegradability. With the proven hemocompatibility, we anticipate that the fabricated smooth and uniform organic–inorganic hybrid LAP-doped PLGA nanofibers may find many tissue engineering applications.

## Acknowledgements

This work is financially supported by High-Tech Research and Development Program of China (2012AA030309), the Program for New Century Excellent Talents in University, State Education Ministry, "111 Project", B07024, and the project PEst-OE/QUI/UI0674/2011 (CQM, Fundação para a Ciência e a Tecnologia (FCT)/Portuguese Government funds for H.T., R.C. and X.S.). S.W. thanks the Innovation Funds of Donghua University Doctorate Dissertation of Excellence (BC201107). X.S. gratefully acknowledges the FCT and Santander bank for the Invited Chair in Nanotechnology. M.Z. thanks the National Natural Science Foundation of China (50925312) for support. Valuable discussion with Dr Chuanglong He is also highly appreciated.

## Notes and references

1 J. Du and Y. L. Hsieh, *Cellulose*, 2009, **16**, 247–260.
2 K. O. Kim, Y. A. Seo, B. S. Kim, K. J. Yoon, M. S. Khil, H. Y. Kim and I. S. Kim, *Colloid Polym. Sci.*, 2011, **289**, 863–870.
3 P. A. Patel, J. Eckart, M. C. Advincula, A. J. Goldberg and P. T. Mather, *Polymer*, 2009, **50**, 1214–1222.
4 D. Sun, J. Yang and X. Wang, *Nanoscale*, 2009, **2**, 287–292.
5 K. Wei, T. Ohta, B. S. Kim, K. W. Kim, K. H. Lee, M. S. Khil, H. Y. Kim and I. S. Kim, *Polym. Adv. Technol.*, 2010, **21**, 746–751.
6 X. Yan, G. Liu, M. Haeussler and B. Z. Tang, *Chem. Mater.*, 2005, **17**, 6053–6059.
7 H. Ma, Y. Huang, M. Shen, R. Guo, X. Cao and X. Shi, *J. Hazard. Mater.*, 2012, **211–212**, 349–356.
8 S. Xiao, H. Ma, M. Shen, S. Wang, Q. Huang and X. Shi, *Colloids Surf., A*, 2011, **381**, 48–54.
9 S. Xiao, M. Shen, R. Guo, Q. Huang, S. Wang and X. Shi, *J. Mater. Chem.*, 2010, **20**, 5700–5708.
10 S. Xiao, M. Shen, R. Guo, S. Wang and X. Shi, *J. Phys. Chem. C*, 2009, **113**, 18062–18068.
11 S. Xiao, M. Shen, H. Ma, X. Fang, Q. Huang, W. J. Weber Jr and X. Shi, *J. Nanosci. Nanotechnol.*, 2011, **11**, 5089–5097.
12 S. Xiao, S. Wu, M. Shen, R. Guo, Q. Huang, S. Wang and X. Shi, *ACS Appl. Mater. Interfaces*, 2009, **1**, 2848–2855.
13 X. Fang, H. Ma, S. Xiao, M. Shen, R. Guo, X. Cao and X. Shi, *J. Mater. Chem.*, 2011, **21**, 4493–4501.
14 Y. Huang, H. Ma, S. Wang, M. Shen, R. Guo, X. Cao and X. Shi, *ACS Appl. Mater. Interfaces*, 2012, **4**, 3054–3061.
15 E. R. Kenawy, G. L. Bowlin, K. Mansfield, J. Layman, D. G. Simpson, E. H. Sanders and G. E. Wnek, *J. Controlled Release*, 2002, **81**, 57–64.
16 R. Qi, R. Guo, M. Shen, X. Cao, L. Zhang, J. Xu, J. Yu and X. Shi, *J. Mater. Chem.*, 2010, **20**, 10622–10629.
17 J. Yun, J. S. Im, Y. S. Lee and H. I. Kim, *Eur. Polym. J.*, 2011, **47**, 1893–1902.
18 M. C. Weisenberger, E. A. Grulke, D. Jacques, A. T. Rantell and R. Andrewsa, *J. Nanosci. Nanotechnol.*, 2003, **3**, 535–539.
19 J. Lee, G. Tae, Y. H. Kim, I. S. Park and S. H. Kim, *Biomaterials*, 2008, **29**, 1872–1879.
20 F. Liu, R. Guo, M. Shen, S. Wang and X. Shi, *Macromol. Mater. Eng.*, 2009, **294**, 666–672.
21 R. Qi, X. Cao, M. Shen, R. Guo, J. Yu and X. Shi, *J. Biomater. Sci., Polym. Ed.*, 2012, **23**, 299–313.
22 V. Guarino, M. Alvarez-Perez, V. Cirillo and L. Ambrosio, *J. Bioact. Compat. Polym.*, 2011, **26**, 144–160.
23 F. Liu, R. Guo, M. Shen, X. Cao, X. Mo, S. Wang and X. Shi, *Soft Matter*, 2010, **8**, 239–253.
24 H. Liao, R. Qi, M. Shen, X. Cao, R. Guo, Y. Zhang and X. Shi, *Colloids Surf., B*, 2011, **84**, 528–535.

 

25 A. Melaiye, Z. Sun, K. Hindi, A. Milsted, D. Ely, D. H. Reneker, C. A. Tessier and W. J. Youngs, *J. Am. Chem. Soc.*, 2005, **127**, 2285–2291.
26 A. Greiner and J. H. Wendorff, *Angew. Chem., Int. Ed.*, 2007, **46**, 5670–5703.
27 L. A. Smith and P. X. Ma, *Colloids Surf., B*, 2004, **39**, 125–131.
28 S. Wang, X. Cao, M. Shen, R. Guo, I. Bányai and X. Shi, *Colloids Surf., B*, 2012, **89**, 254–264.
29 X. Lu, C. Wang and Y. Wei, *Small*, 2009, **5**, 2349–2370.
30 Y. Zhao, S. Wang, Q. Guo, M. Shen and X. Shi, *J. Appl. Polym. Sci.*, 2012, DOI: 10.1002/app.38054.
31 S. Xiao, M. Shen, H. Ma, R. Guo, M. Zhu, S. Wang and X. Shi, *J. Appl. Polym. Sci.*, 2010, **116**, 2409–2417.
32 W. K. Son, J. H. Youk, T. S. Lee and W. H. Park, *Macromol. Rapid Commun.*, 2004, **25**, 1632–1637.
33 Y. Zhang, Z. M. Huang, X. Xu, C. T. Lim and S. Ramakrishna, *Chem. Mater.*, 2004, **16**, 3406–3409.
34 D. Li and Y. Xia, *Adv. Mater.*, 2004, **16**, 1151–1170.
35 Y. Li, D. Maciel, H. Tomás, J. Rodrigues, H. Ma and X. Shi, *Soft Matter*, 2011, **7**, 6231–6238.
36 A. K. Gaharwar, P. Schexnailder, V. Kaul, O. Akkus, D. Zakharov, S. Seifert and G. Schmidt, *Adv. Funct. Mater.*, 2010, **20**, 429–436.
37 Q. Jin, P. Schexnailder, A. K. Gaharwar and G. Schmidt, *Macromol. Biosci.*, 2009, **9**, 1028–1035.
38 P. J. Schexnailder, A. K. Gaharwar, R. L. Bartlett Ii, B. L. Seal and G. Schmidt, *Macromol. Biosci.*, 2010, **10**, 1416–1423.
39 V. K. Daga, M. E. Helgeson and N. J. Wagner, *J. Polym. Sci., Part B: Polym. Phys.*, 2006, **44**, 1608–1617.
40 X. Xin, M. Hussain and J. J. Mao, *Biomaterials*, 2007, **28**, 316–325.
41 H. Hosseinkhani, M. Hosseinkhani, F. Tian, H. Kobayashi and Y. Tabata, *Biomaterials*, 2006, **27**, 4079–4086.
42 S. Y. Jeon, J. S. Park, H. N. Yang, D. G. Woo and K. H. Park, *Biomaterials*, 2012, **33**, 4413–4423.
43 M. Bosetti, F. Boccafoschi, M. Leigheb, A. E. Bianchi and M. Cannas, *J. Tissue Eng. Regener. Med.*, 2012, **6**, 205–213.
44 X. Hu, S. H. Park, E. S. Gil, X. X. Xia, A. S. Weiss and D. L. Kaplan, *Biomaterials*, 2011, **32**, 8979–8989.
45 H. Y. Huang and Q. Q. Tang, *Stem Cells and Cancer Stem Cells*, 2012, **6**, 205–211.
46 Y. Kohl, E. Gorjup, A. Katsen-Globa, C. Büchel, H. von Briesen and H. Thielecke, *J. Nanopart. Res.*, 2011, **13**, 6789–6803.
47 C. P. Zhao, C. Zhang, Y. H. Wang, S. N. Zhou, C. Zhou, W. Y. Li and M. J. Yu, *Cell Biol. Int.*, 2007, **31**, 1428–1435.
48 A. Martins, A. R. C. Duarte, S. Faria, A. P. Marques, R. L. Reis and N. M. Neves, *Biomaterials*, 2010, **31**, 5875–5885.
49 H. M. Kelly, P. B. Deasy, E. Ziaka and N. Claffey, *Int. J. Pharm.*, 2004, **274**, 167–183.
50 S. Jabbari-Farouji, H. Tanaka, G. H. Wegdam and D. Bonn, *Phys. Rev. E: Stat., Nonlinear, Soft Matter Phys.*, 2008, **78**, 061405.
51 Z. X. Meng, W. Zheng, L. Li and Y. F. Zheng, *Mater. Sci. Eng., C*, 2010, **30**, 1014–1021.
52 S. Wang, S. Wen, M. Shen, R. Guo, X. Cao, J. Wang and X. Shi, *Int. J. Nanomed.*, 2012, **6**, 3449–3459.
53 H. Wu, G. Liu, Y. Zhuang, D. Wu, H. Zhang, H. Yang, H. Hu and S. Yang, *Biomaterials*, 2011, **32**, 4867–4876.
54 Y. Imai and Y. Nose, *J. Biomed. Mater. Res.*, 1972, **6**, 165–172.
55 S. Perrot, H. Dutertre-Catella, C. Martin, P. Rat and J. M. Warnet, *Toxicol. Sci.*, 2003, **72**, 122–129.
56 N. N. Herrera, J.-M. Letoffe, J.-L. Putaux, L. David and E. Bourgeat-Lami, *Langmuir*, 2004, **20**, 1564–1571.
57 L. F. Fernandes, M. A. Costa, M. H. Fernandes and H. Tomás, *Connect. Tissue Res.*, 2009, **50**, 336–346.
58 H. M. da Silva, M. Mateescu, C. Damia, E. Champion, G. Soares and K. Anselme, *Colloids Surf., B*, 2010, **80**, 138–144.
59 Y. Huang, X. Jin, X. Zhang, H. Sun, J. Tu, T. Tang, J. Chang and K. Dai, *Biomaterials*, 2009, **30**, 5041–5048.
60 G. Kumar, C. K. Tison, K. Chatterjee, P. S. Pine, J. H. McDaniel, M. L. Salit, M. F. Young and C. G. Simon Jr, *Biomaterials*, 2011, **32**, 9188–9196.
61 J. S. Sun, W. H. S. Chang, L. T. Chen, Y. C. Huang, L. W. Juang and F. H. Lin, *Biomaterials*, 2004, **25**, 607–616.